9B.5 INTERANNUAL VARIATIONS OF SURFACE RADIATION BUDGET

Pamela E. Mlynczak*
Science Systems and Applications, Inc., Hampton, VA

G. Louis Smith
National Institute of Aerospace, Hampton, VA

Paul W. Stackhouse, Jr.
NASA Langley Research Center, Hampton, VA

ABSTRACT

The NASA/GEWEX Surface Radiation Budget (SRB) data set covers the 22-year period from July 1983 through June 2005. The interannual variations of shortwave downward flux (SWN), longwave upward flux (LWU) and longwave downward flux (LWD) at the surface are computed using the monthly means. Variations of SWN are due to variations of cloud, whereas variations of LWU are due to variations of surface temperature. Variations of LWD can be due to variations in fraction of coverage and altitude of clouds and to variations of atmospheric temperature and humidity. Whereas the diurnal and annual cycles of radiation components are due to cycles of insolation, interannual variations are due to free variations of the coupled cryosphere-ocean-atmosphere-land system.

The root-mean-squares of the interannual variations are 14.4 W m^{-2} for SWN, 6.8 W m^{-2} for LWU, and 7.3 W m^{-2} for LWD. A principal component analysis was performed on each component. The variances for the principal components decrease slowly with order following a power law. For SWN, the largest principal component describes the El Nino. The next term shows a definite trend of increasing SWN over the data period. Artifacts of the data set appear in higher order principal components. Current research is examining the relation of the principal components to interannual variations of other processes.

1. INTRODUCTION

The purpose of this paper is to examine the global distribution of interannual variations of surface radiation fluxes, namely shortwave net flux (SWN), longwave upward flux (LWU), and longwave downward flux (LWD). To that end, principal component analysis will be used to compute the temporal and spatial aspects of these variations. Not only will global values of interannual variations be found, smaller regions of interest, in either space or time, will be identified for further study.

The NASA/GEWEX Surface Radiation Budget Data Set (Gupta et al. 2006; Cox et al. 2006) will be used because it provides global coverage of the surface radiation fluxes for more than two decades. Longwave fluxes are obtained from SRB Release 2.5, and shortwave fluxes are obtained from SRB Release 3.0. The surface fluxes are based on cloud cover information provided by the International Satellite and Cloud Climatology Program (ISCCP) DX data (Rossow and Schiffer 1991) and on Goddard Earth Observing System Data Assimilation System-4 (GEOS-4) reanalysis data that describe the surface and atmospheric temperature and humidity. Monthly mean fluxes for a 22-year period from July 1983 to June 2005 are used. The data set is on a quasi-equal area grid with one-degree resolution in both latitude and longitude at the Equator. (The SRB data set is available at http://eosweb.larc.nasa.gov/PRODOCS/srb/table_srb.html.)

In order to study the interannual variations of the 64,800 regions that cover the globe at one-degree equal angle resolution, a principal component analysis (PCA) is used. The principal components (PCs) describe the variations in time, and their corresponding empirical orthogonal functions (EOFs) describe the strength of each PC at each region. The analysis method will first be described, followed by PCA results from the global study of SWN, LWU and LWD. Finally, results from a PCA of a smaller area over the South Atlantic Convergence Zone (SACZ) will be shown.

2. ANALYSIS METHOD

The SRB data set has 44016 regions on its quasi-equal area grid, with monthly mean values of surface downward and upward shortwave and longwave fluxes. SWN is computed from the downward and upward shortwave fluxes. The flux values are regridded onto a 360° by 180° equal angle grid (64800 regions) using replication. The climatological monthly means for each calendar month are then computed for the period July 1983 through June 2005, which includes 264 months. Then, for any given region, the interannual variations over the period are calculated by taking the difference between that region's 264 monthly mean flux values and their associated climatological monthly means. Another way to look at this is that a region's monthly mean flux values equal the sum of three things: the climatological annual mean, the annual cycle about that mean, and the interannual variations. The annual cycle is quite stable and mainly forced by the annual cycle of insolation at TOA, but the interannual variations include any other oscillations in the system from month to month and year to year. This study is focused on these interannual variations.

*Corresponding author address:
Pamela E. Mlynczak, SSAI, 1 Enterprise Parkway, Suite 200, Hampton, VA 23666.
E-mail: Pamela.E.Mlynczak@nasa.gov

In order to quantify the interannual variations for all 64800 regions, principal component analysis is used. The first step is to form a covariance matrix as

$$\Gamma(m,m') = \sum_{x=1}^{64800} w(x)V(x,m)V(x,m'),$$

where $V(m,x)$ denotes the interannual variations at month m for region x and $w(x)$ is the area weighting for region x. Since there are 264 months in this study, the covariance matrix is 264x264. The principal components of this covariance matrix Γ are the eigenvectors $PC_n(m)$ where $n \in [1,264]$. They describe the temporal pattern in the interannual variations, and the eigenvalues λ_n represent the variance explained by each PC. For each flux, the 264 PCs are projected onto the original 264 monthly mean maps to obtain the empirical orthogonal functions $EOF_n(x)$, giving the spatial coefficients associated with each PC. Thus the interannual variations of a flux at month m and region x can be represented by

$$V(x,m) = \sum_{n=1}^{264} PC_n(m)EOF_n(x).$$

3. GLOBAL TIME AND SPACE VARIATIONS

3.1 Variability Comparison

For surface radiation budget, the net shortwave radiation flux (SWN) is of primary interest because it is the amount of solar radiation absorbed at the surface. Then the longwave upward flux (LWU) provides a measure of the heating at the surface. Longwave downward flux (LWD) is consequently due to the heating from both the atmosphere and the clouds. Figure 1 (Trenberth et al. 2009) illustrates the global annual mean energy budget, at the surface and top of

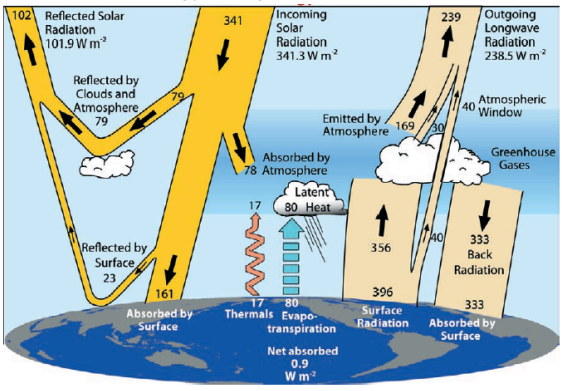

Figure 1. The global annual mean Earth's energy budget for the Mar 2000 to May 2004 period (W m^{-2}). The broad arrows indicate the schematic flow of energy in proportion to their importance.

atmosphere. The magnitudes of the interannual variations of SWN, LWU, and LWD can be put into context when they are compared to the annual mean values and annual cycles of these surface fluxes. Table 1 contains the global annual mean of the three fluxes (from Figure 1) as well as the total root-mean-square (RMS) variances of the annual cycle and interannual variations and their percentages of the global annual mean. The RMS of the interannual variations of SWN is nearly 9% of the annual mean of SWN, whereas the RMS values for both longwave fluxes are approximately 2% of their respective means.

	SWN	LWU	LWD
Global Annual Mean (W m^{-2})	161	396	333
RMS of Annual Cycle (W m^{-2})	50.4	27.4	23.0
% of Global Annual Mean	31.3	6.9	6.9
RMS of Interannual Variations (W m^{-2})	14.4	6.8	7.3
% of Global Annual Mean	8.9	1.7	2.2
RMS(1) (W m^{-2})	3.91	2.16	1.92
λ_1 (normalized eigenvalue)	0.0740	0.1001	0.0685

Table 1. For SWN, LWU and LWD, the global annual mean, the RMS of the annual cycle and its percent of the global annual mean, the RMS of the interannual variations and its percent of the global annual mean, the RMS of PC-1 of the interannual variability, and the normalized eigenvalue of, or fraction of variance explained by, PC-1.

3.2 Importance of Principal Components

In principal component analysis, each PC_nxEOF_n product (combination) describes a portion of the overall temporal and spatial variation in the analyzed parameter. The eigenvalues of the covariance matrix have been normalized to represent the fraction of variance associated with each PC, and so they can be used to determine how important each PC is to explaining the variability in the parameter. The first PC describes the maximum amount of variance that can be represented with one function, with each successive PC describing the maximum amount of variance left in the residual. Figure 2 shows this fraction of variance in the interannual variability for the first 40 PCs in this study.

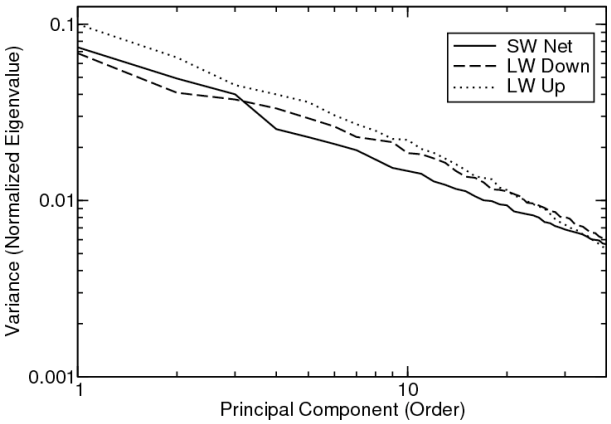

Figure 2. The fraction of variance explained by the first 40 principal components of SWN, LWD, and LWU.

All of the variances are small, with PC-1 explaining 10% of the variance of the SWN interannual variability and only about 7% of the variance of both the LWU and LWD interannual variability. The variances decrease slowly and their logarithms decrease nearly linearly with respect to the logarithm of the principal component order.

Since the variances explained by PCs are small and not well separated, the question arises as to how many of these PCs may be valid. The North et al. (1982) criterion compares the eigenvalue sampling errors to the spacing between adjacent eigenvalues. When the sampling error is larger than the spacing, that PC may have become mixed and may no longer represent just one mode of variation in the interannual variability. Figure 3 shows the sampling errors and eigenvalue spacing for the first ten PCs of SWN. By PC-4 and PC-5, the error is as large as the spacing, and so these

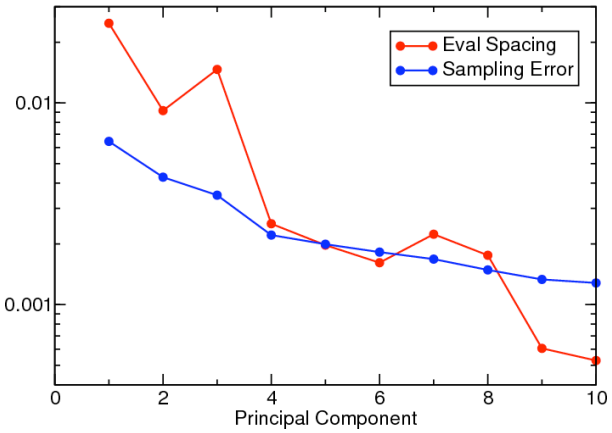

Figure 3. Sampling errors and spacing between successive eigenvalues of the PCA of SWN.

PCs cannot be considered to represent separate modes. Although the patterns may be mixed, the value of these lower order PCs cannot be disregarded because the corresponding EOF maps indicate active regions of interannual variability, as will be shown.

3.3 Principal Component Analysis of Shortwave Net

Table 1 shows that the global annual mean SWN is 161 W m^{-2}, and Figure 4 shows the geographical distribution of this mean. The North African desert is reflecting SW back to space, thereby reducing SWN at the surface. Subsidence regions over the tropical and subtropical oceans have the largest mean SWN because they have fewer clouds than surrounding areas. The annual cycle has a global RMS of 50.4 W m^{-2} and is discussed by Wilber et al. (2006), and the interannual variations have a global RMS of 14.4 W m^{-2}. The geographical distribution of the RMS of interannual variations is shown in Figure 5. The interannual variations have the most variability across the equatorial Pacific Ocean and tropical Indian Ocean.

The first PC of SWN interannual variations is shown in Figure 6 as a function of time, and the fraction of total variance it explains is 7.4% (Table 1). Since the PCs carry the units in this analysis, they show the magnitude of the flux's interannual variations. PC-1 has a range of 21 W m^{-2} over the analysis period. Figure 7a shows EOF-1 for SWN, the geographical coefficients that correspond to PC-1. The ENSO pattern is clearly represented in SWN EOF-1, but artifacts due to satellite changes and coverage boundaries can also be seen. For example, the region centered over the Indian Ocean did not have satellite coverage until 1998. EOF-2 in Figure 7b also clearly shows this gap over the Indian Ocean as well as the boundary between GOES-East

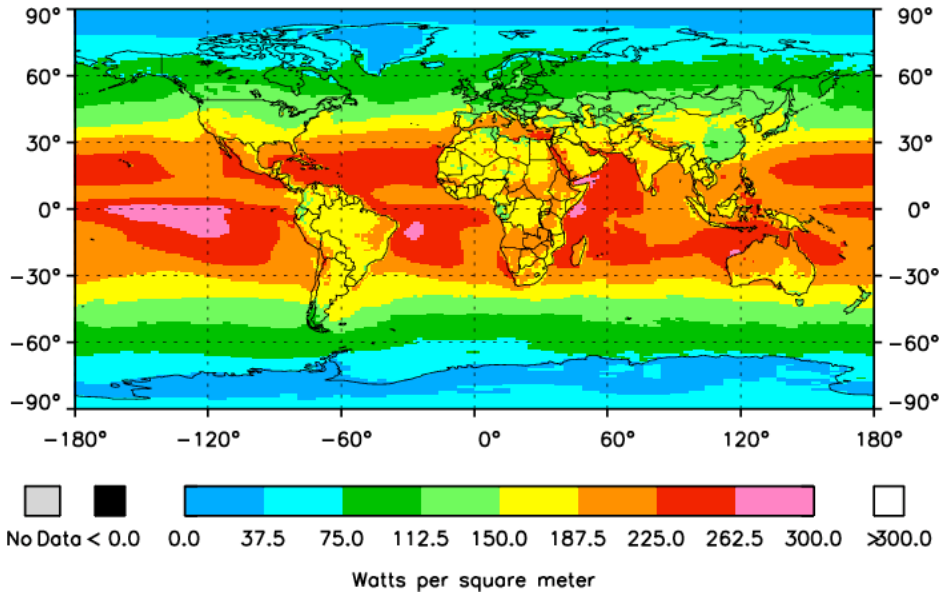

Figure 4. Annual mean SWN flux in W m^{-2}.

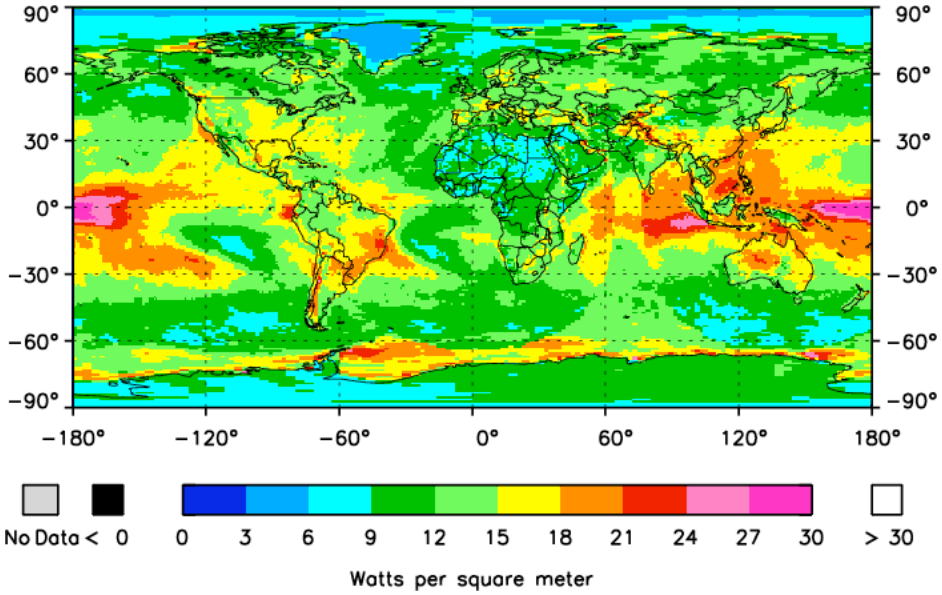

Figure 5. RMS of interannual variations of SWN in W m^{-2}.

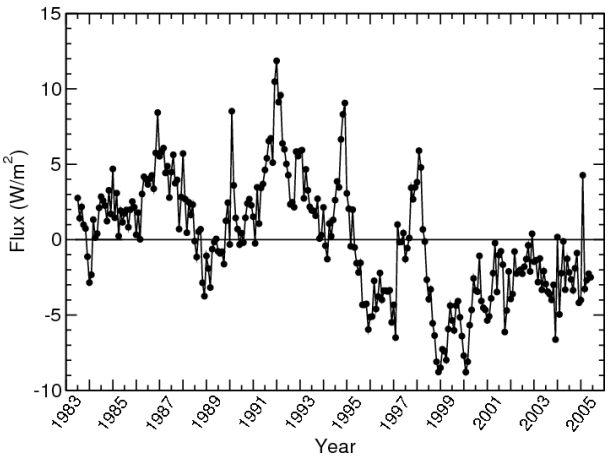

Figure 6. First principal component of the SWN interannual variations in W m^{-2}.

and the Meteosat satellites. The north-south variations of the ENSO pattern are described by EOF-3 (Figure 7c). Figure 7d shows EOF-4, which contains a pattern of Indian Ocean activity as well as variations over the equatorial Pacific. The time series associated with EOF-4 is PC-4, shown in Figure 8. This PC-4 plot is typical of many of the PCs for SWN interannual variations; they appear to be noisy, but they contain useful information about the magnitude of the variability. EOF-8 for SWN is shown in Figure 9. Based on the North criterion, PC-8 and thus EOF-8 is a mix of patterns (Figure 2), but EOF-8 shows an interesting feature in the SWN variations in the region of the South Atlantic Convergence Zone that will be addressed later in this paper.

EOFs 4-9 all show patterns of SWN interannual variability over the Indian Ocean. A possible reason for this variability includes the MJO, which initiates in this region with deep convective activity and which has a period of 40-60 days that can alias into the monthly means. Other potential contributors to the variability in SWN include the variability of the Indian monsoons, the Indian Ocean dipole, and artifacts due to spacecraft changes.

Many studies of interannual variability have focused on pressure height change, which is a suitable technique for extratropical regions. The SWN flux record has an advantage for looking at interannual variability at low latitudes, however. Near the Equator, the lack of Coriolis force results in small variations in pressure heights, so that in the tropics, variations in SWN are more sensitive to processes than are the pressure heights.

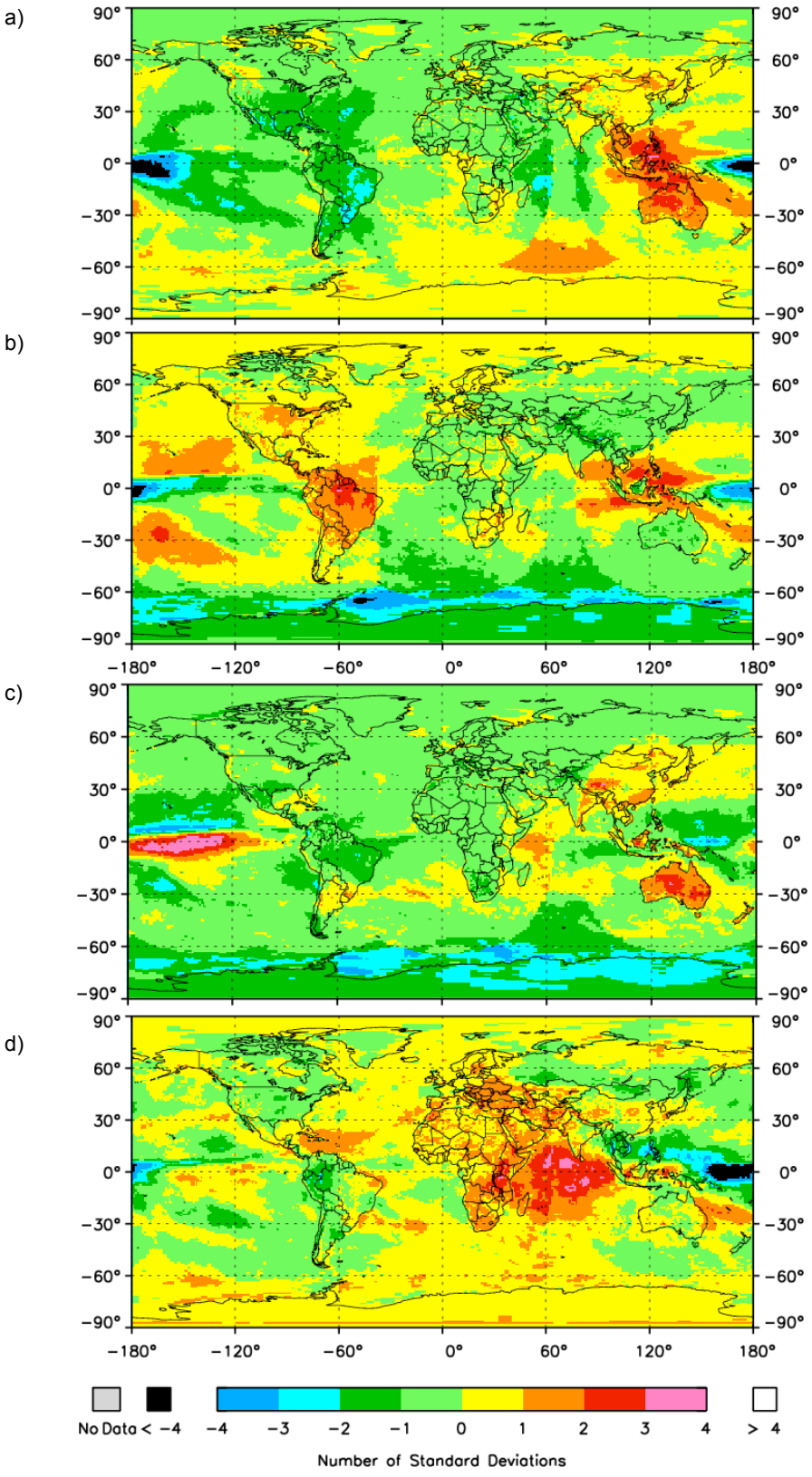

Figure 7. First four EOFs of SWN interannual variations a) EOF-1 b) EOF-2 c) EOF-3 d) EOF-4.

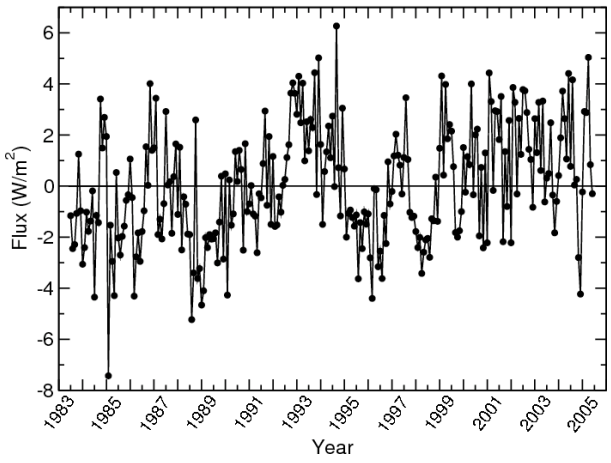

Figure 8. PC-4 of SWN interannual variations in W m^{-2}.

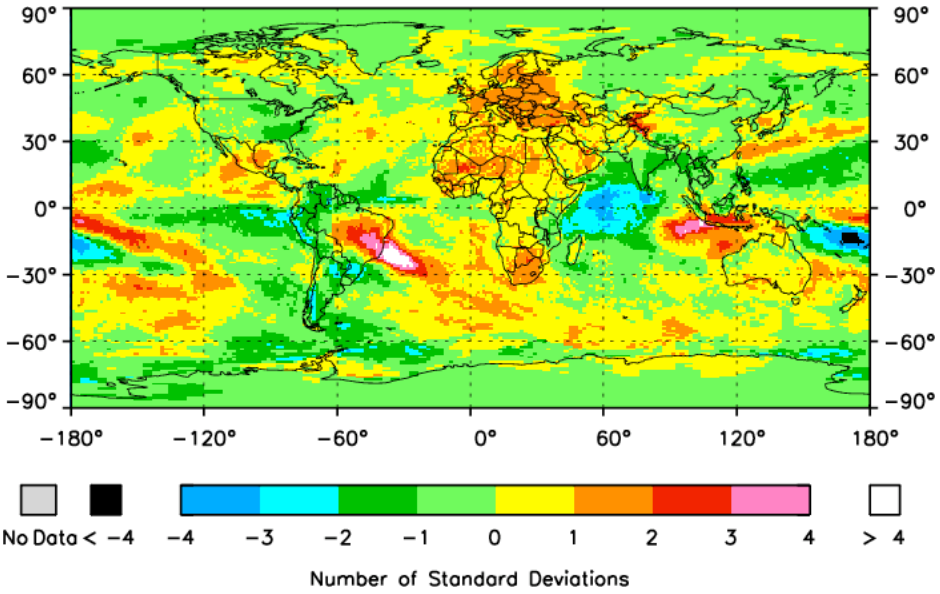

Figure 9. EOF-8 of SWN interannual variations.

3.4 Principal Component Analysis of Longwave Upward

The surface's response to heating from the sun is LWU. The global annual mean of LWU is 396 W m^{-2} (Table 1), and Figure 10 shows the geographical distribution of this mean, which is reasonably zonal in nature. Note that regions of higher elevation, like the Tibetan Plateau, the Andes and the Rocky Mountains, have colder surface temperatures and thus less LWU. The annual cycle of LWU has a global RMS value of 27.4 W m^{-2}, and the global RMS of the interannual variations is 6.8 W m^{-2}. The map of the RMS of LWU interannual variations is shown in Figure 11. Desert regions and high latitude regions have RMS values greater than 10 W m^{-2}, but the oceans have little variability.

Figure 12 shows the first PC of LWU interannual variations, and it explains 10% of the total variance (Table 1). This first mode also has a RMS of 2.16 W m^{-2}, which is roughly a third of the total RMS of interannual variability. There is a large jump from positive to negative values in 2001 due to a change in the TOVS (TIROS Operational Vertical Sounder) algorithm. This change increased surface temperatures and is reflected in the ISCCP data from which the NASA/GEWEX SRB algorithms obtain skin temperature. EOF-1 for LWU is shown in Figure 13 and displays a strong variability in LWU over North Africa, the Middle East, and southwest Asia, as well as other desert regions. When the negative values in the PC-1 time series are multiplied by their corresponding negative EOF-1 coefficients, an increase in LWU occurs. The ENSO signal across the equatorial Pacific is described by EOF-3 (Figure 14), and PC-3 (Figure 15) shows a strong signature during the 1997-1998 ENSO event.

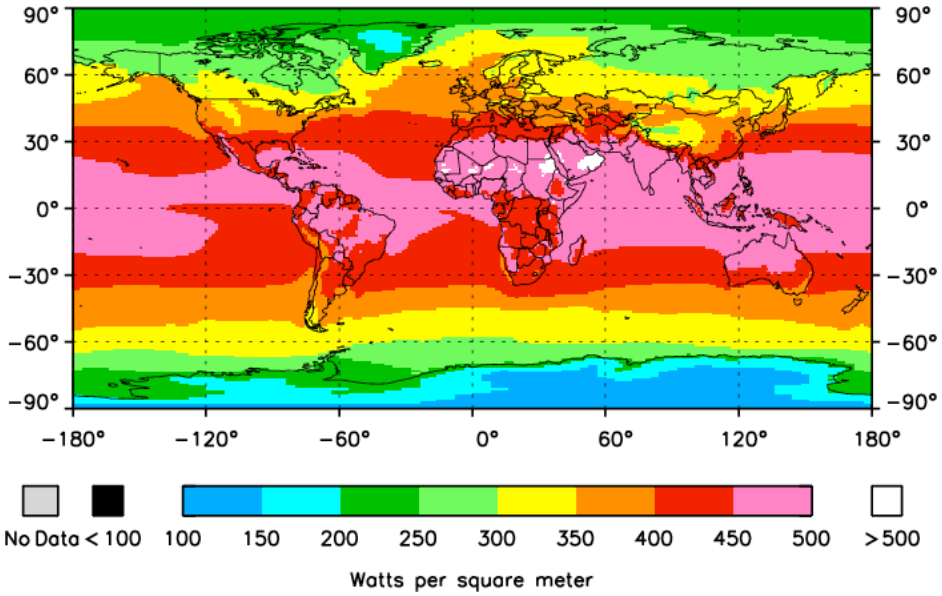

Figure 10. Annual mean LWU flux in W m^{-2}.

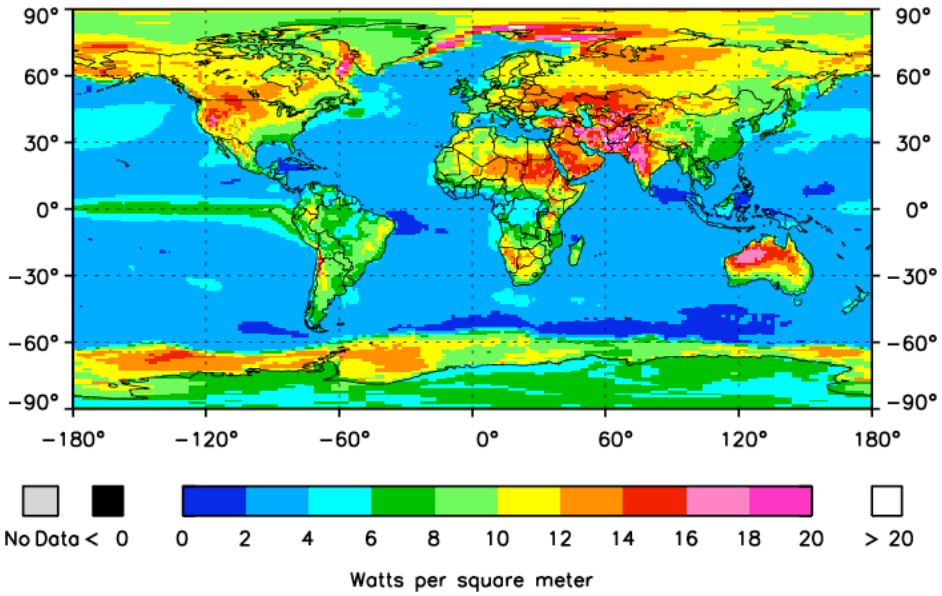

Figure 11. RMS of LWU interannual variations in W m^{-2}.

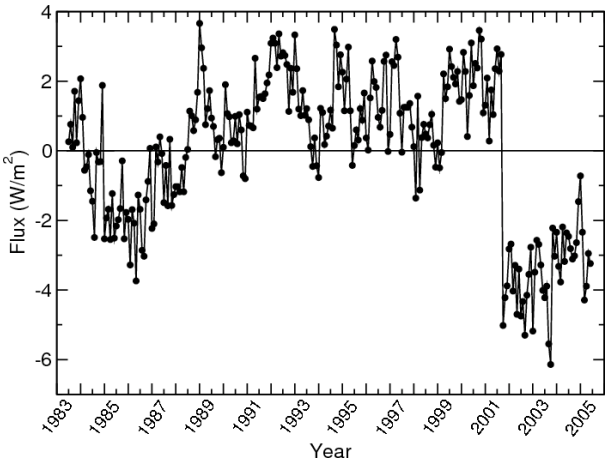

Figure 12. PC-1 of LWU interannual variations in W m^{-2}.

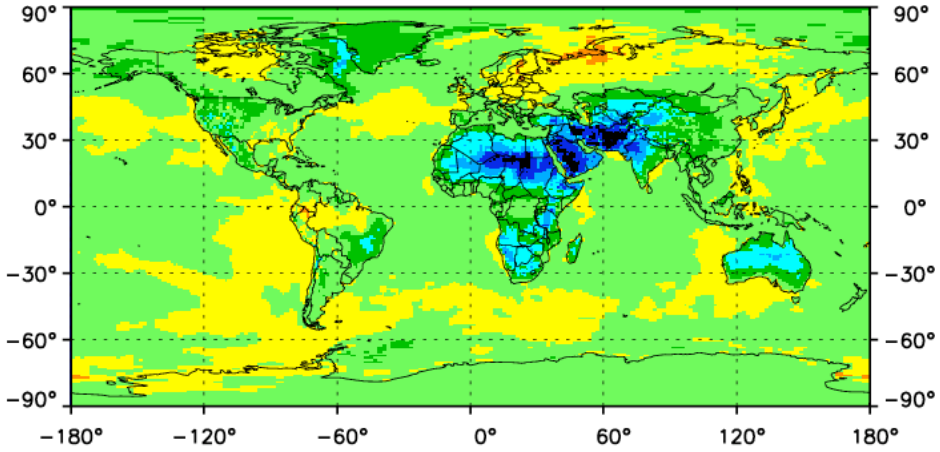

Figure 13. EOF-1 of LWU interannual variations.

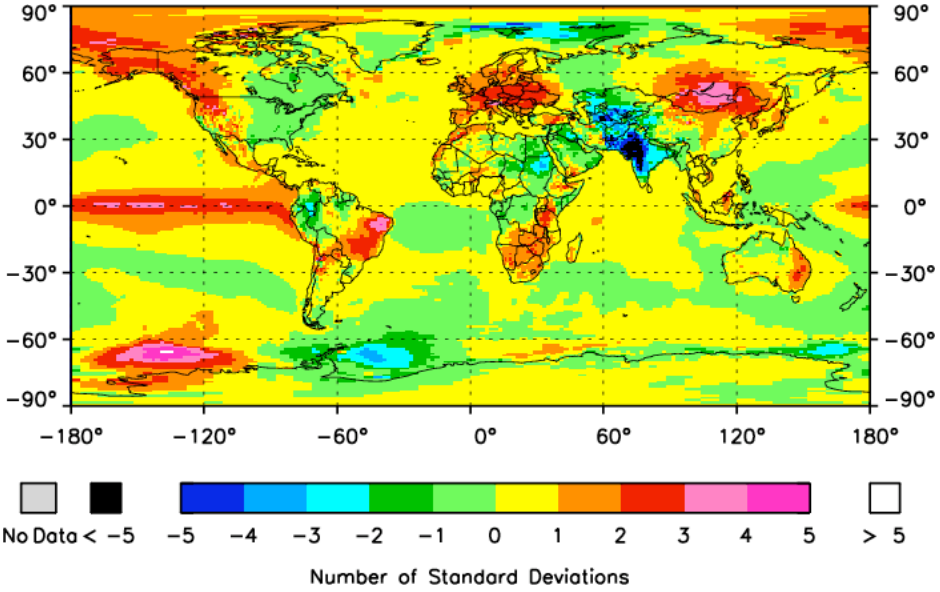

Figure 14. EOF-3 of LWU interannual variations.

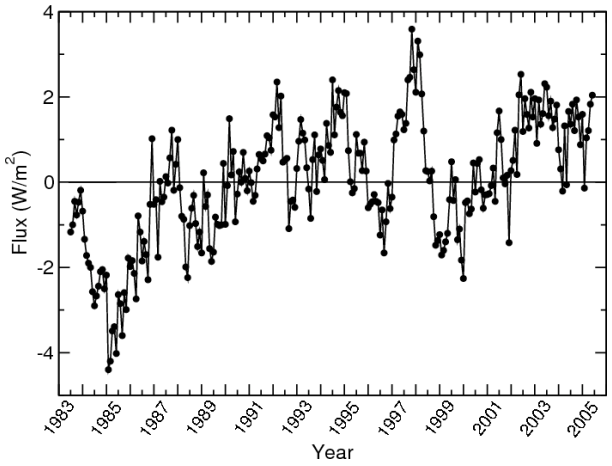

Figure 15. PC-3 of LWU interannual variability in W m^{-2}.

3.5 Principal Component Analysis of Longwave Downward

The atmosphere reacts to being heated by radiating some of that heat back to the surface. Table 1 shows that the global annual mean of LWD is 333 W m^{-2}, and the geographical distribution of that mean is shown in Figure 16. The patterns in LWD are similar to those in LWU except for desert regions where low humidity reduces LWD. This demonstrates that the atmospheric temperature is closely coupled with that of the surface. The RMS of the annual cycle of LWD is 23.0 W m^{-2}, and the global RMS of the interannual variations is 7.3 W m^{-2}. Figure 17 shows the distribution of the RMS of LWD, with patterns that are quite similar to those of the RMS for LWU.

The first PC of LWD interannual variations is shown in Figure 18, and it explains less than 2% of the variance (Table 1). This time series has a strong signal during the 1997-98 ENSO event, and the ENSO pattern can be seen in the corresponding geographical distribution of PC-1, which is EOF-1 (Figure 19). PC-3 and EOF-3 (Figures 20 and 21) also illustrate ENSO, and EOF-3 shows large variability in the interannual variations of LWD over Australia and Canada. EOF-6 (Figure 22) shows that for LWD, variations are more prominent at high latitudes. At low latitudes, high humidity in the PBL may mitigate variations, and at higher latitudes, the varying nature of stratiform clouds may increase variations in LWD.

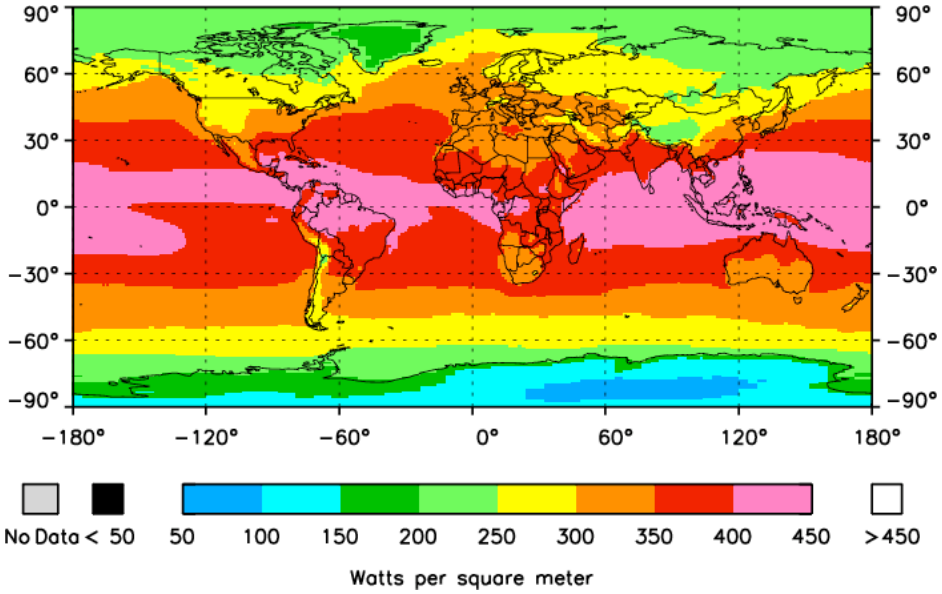

Figure 16. Annual mean LWD flux in W m^{-2}.

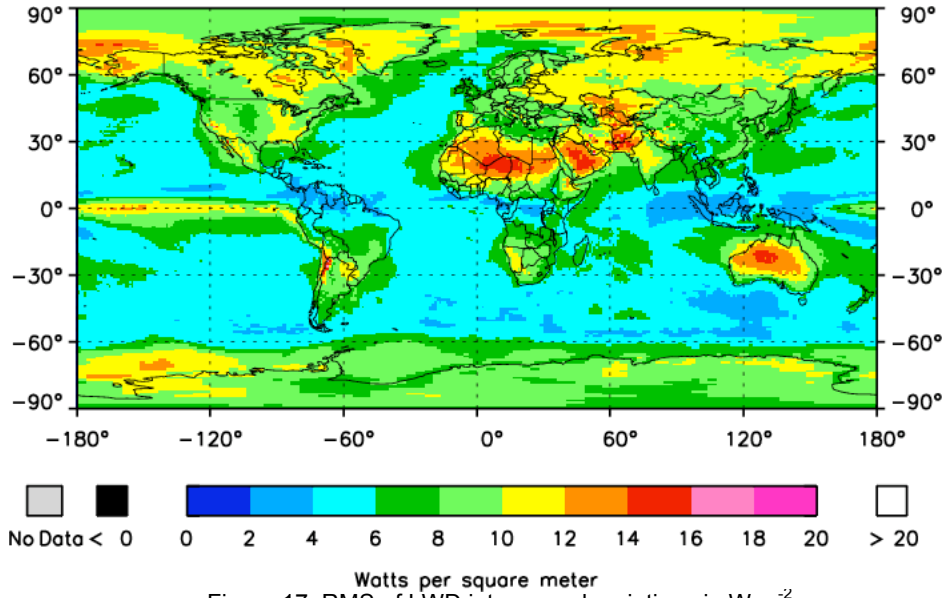

Figure 17. RMS of LWD interannual variations in W m^{-2}.

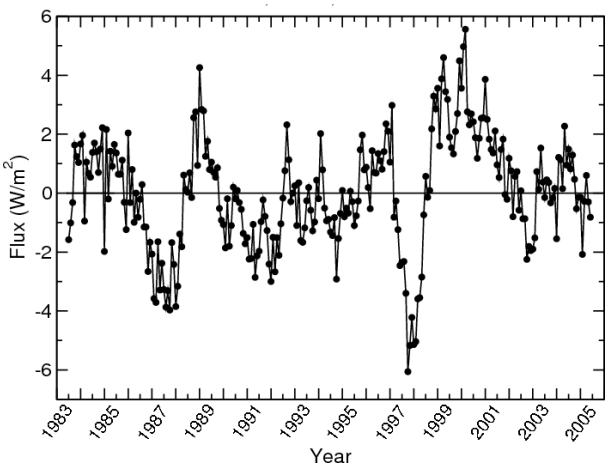

Figure 18. PC-1 of LWD interannual variations in W m^{-2}.

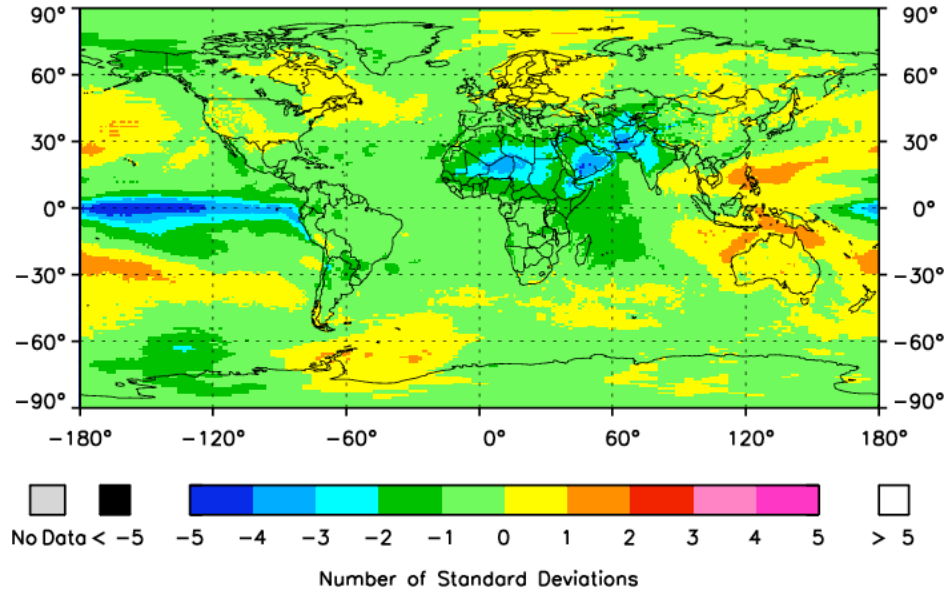

Figure 19. EOF-1 of LWD interannual variations.

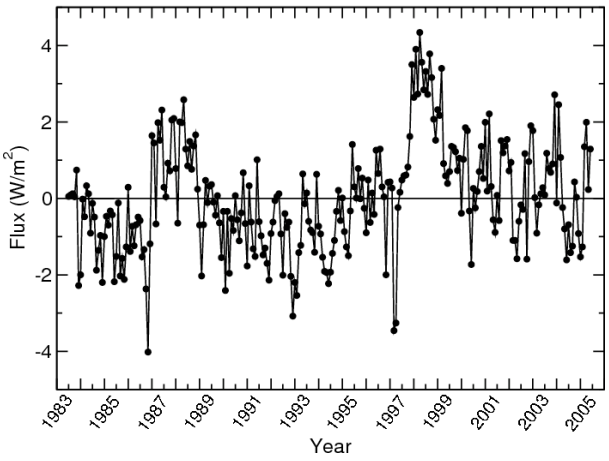

Figure 20. PC-3 of LWD interannual variations in W m^{-2}.

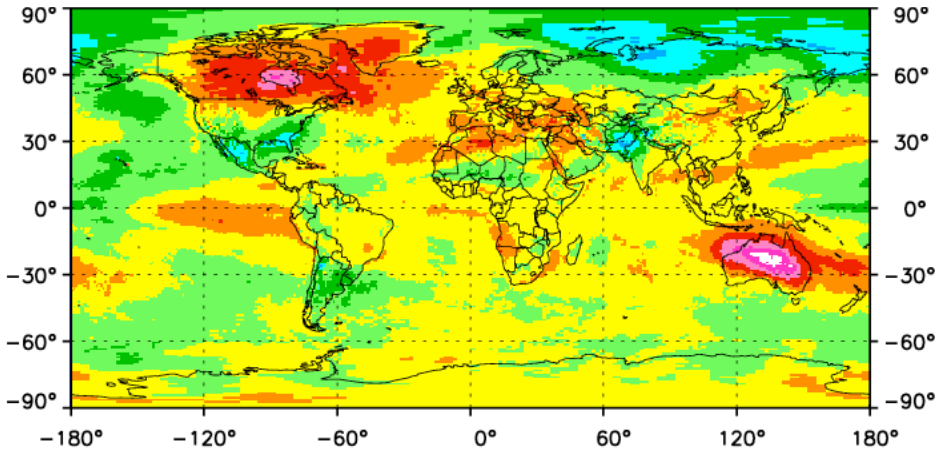

Figure 21. EOF-3 of LWD interannual variations.

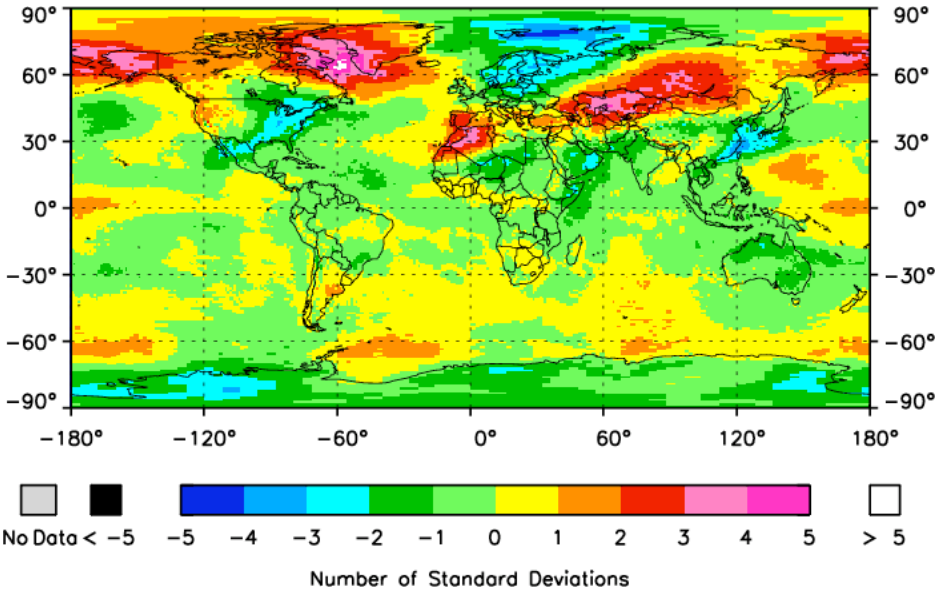

Figure 22. EOF-6 of LWD interannual variations.

4. REGIONAL TIME AND SPACE VARIATIONS

EOF-8 of the global analysis of SWN, shown in Figure 9, has an interesting feature over the South Atlantic Convergence Zone (SACZ). The North criterion suggests that the solutions are mixed at this order, so a PC analysis is performed on this restricted region to learn more about this feature. The global analysis showed that for EOF-8 of SWN, the interannual variations were some of the largest during the month of December. Figure 23 shows the December monthly mean of SWN. The light and dark pink regions indicate clear sky where large amounts of SW are being absorbed at the surface. Over Brazil, SWN is greatly reduced, illustrating deep convection. There is convergence over the region, uplift, cloud formation, and then outflow to the southeast over the Atlantic Ocean. This region is indicated with orange in the figure.

For this restricted analysis region the first principal component explains 15.2% of the total variance in the SWN interannual variability, and PC-2 explains 7.8%. The total RMS of SWN interannual variability is 14.6 W m^{-2}, which is nearly the same as the value for the global analysis. Figure 24 shows the first two EOFs, the spatial distributions of the first two PCs. These maps illustrate the convective feature clearly. EOF-1 in Figure 24a shows the variation from year to year of convective activity over the continent, while EOF-2 in Figure 24b shows the variation in the position of the outflow of clouds from the convective region. The boundary between GOES-East and Meteosat can also be seen in EOF-1.

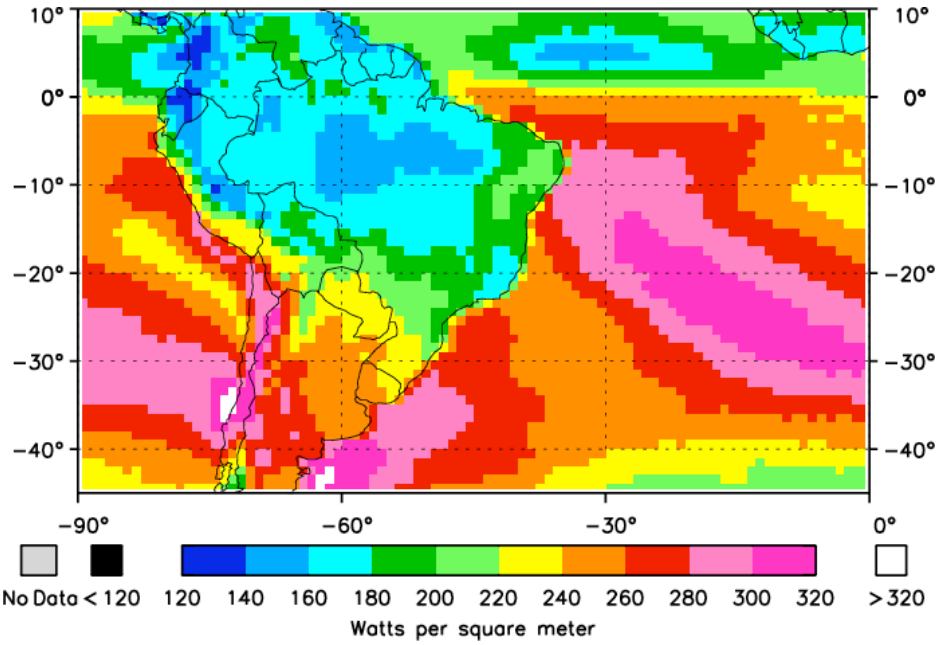

Figure 23. December monthly mean of SWN flux in W m^{-2} over the SACZ.

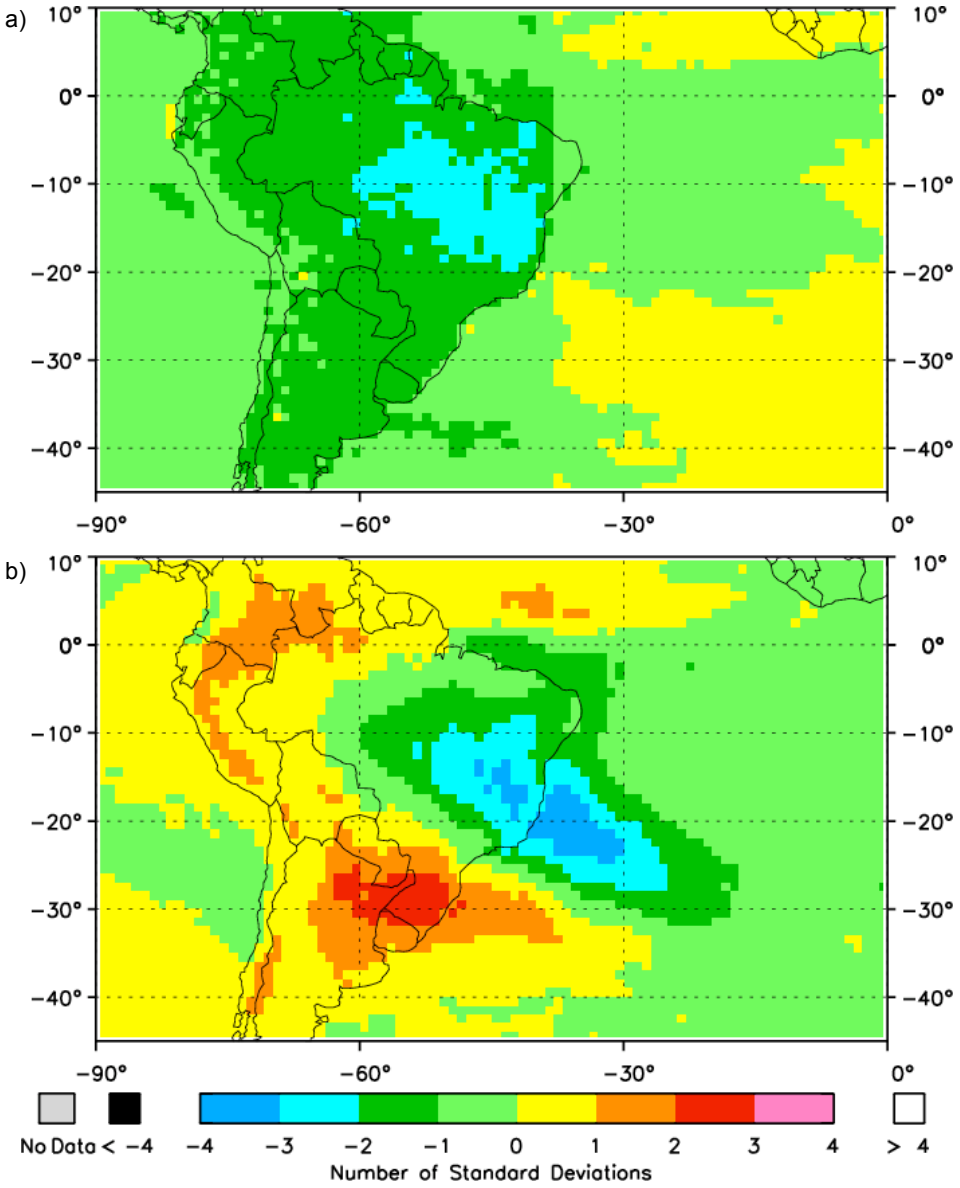

Figure 24. First two EOFs of SWN interannual variations over the SACZ a) EOF-1 b) EOF-2.

5. DISCUSSION

Examination of the various EOF maps and their PCs helps to identify regions and modes of prominent interannual variability. Table 2 summarizes areas of interest in the interannual variability of SWN for the first eight PCs. As previously seen in Figure 7, one major effect in the EOF maps is ENSO. Artifacts due to spacecraft changes also appear, and it is important to understand the presence of these artifacts and what they contribute to the variability in the SRB dataset. There is large SWN interannual variability over the Indian Ocean as well. Figure 9 showed an interesting feature in the interannual variability of SWN over the SACZ. Further investigation of this region alone showed that the feature was indeed real and not an artifact of

PC	Major Areas
1	ENSO
2	Artifact due to spacecraft
3	ENSO North-South variation
4	Indian Ocean activity
5	Indian Ocean activity
6	Indian Ocean activity
7	Equatorial and Subtropical Pacific
8	SACZ

Table 2. For SWN, the major regions or effects of interannual variability associated with PC-1 through PC-8.

the PCA. Table 3 includes major effects seen in the interannual variability of LWU. Perhaps not surprisingly,

PC	Major Areas
1	North Africa, Saudi Arabia, SW Asia
2	North Africa, Southern Asia, Australia
3	ENSO and Eurasia
4	North America and Asia
5	ENSO, North America, Asia
6	High Latitudes North
7	High Latitudes North
8	Eurasia Dipole

Table 3. For LWU, the major regions or effects of interannual variability associated with PC-1 through PC-8.

regions with hot deserts showed prominent variability in the first two PCs. ENSO features are found in PC-3 and PC-5, while other areas of LWU variability are found in the higher latitudes of the Northern Hemisphere. Areas of interest in the LWD interannual variability are listed in Table 4. Once again, ENSO is a major feature, as

PC	Major Areas
1	ENSO and North Africa
2	North Africa, Eastern Russia, Eq. Pacific
3	Canada and Australia
4	North America and Eurasia
5	High Latitudes North and South
6	High Latitudes North
7	High Latitudes North and North Africa
8	Canada and Australia

Table 4. For LWD, the major regions or effects of interannual variability associated with PC-1 through PC-8.

shown by both EOF-1 and EOF-3 of LWD (Figures 19 and 21). Other areas of variability include North Africa, North America, and Australia. In general, the interannual variability in LWD is higher at higher latitudes than at lower latitudes.

The North criterion shows that there are about four discernable modes of interannual variability in SWN, LWU and LWD. Although the modes may be mixed in higher orders, these PCs and EOFs are still valuable because they provide clues for further investigation. These PCs and EOFs illustrate variations that may be better understood with PCA on restricted regions as opposed to global PCA.

6. CONCLUDING REMARKS

Some questions arise from this exploratory study. For example, why are SW variations large at low latitudes while LW variations are more prominent at higher latitudes? How valid are the results of this PCA? Do errors in the PCA outweigh any physical mechanisms behind the variability that has been described? Future research is needed to find answers to these questions and to better understand the interannual variability of these three important surface fluxes. The effects of changes in the observing system need to be understood and quantified. The effect of the TOVS algorithm changes on the ISCCP skin temperatures needs to be evaluated to determine ultimately how the LWU fluxes are affected. Other regions identified in Tables 2 to 4 can be studied with PCA and rotated PCA.

7. ACKNOWLEDGEMENTS

The authors gratefully acknowledge support by the Surface Radiation Budget Program from the NASA Science Mission Directorate through Langley Research Center to Science Systems and Applications Inc. and to the National Institute of Aerospace. They also acknowledge the Atmospheric Sciences Data Center of Langley Research Center for access to the NASA/GEWEX SRB data set.

8. REFERENCES

Cox, S. J., Stackhouse, P. W., S. K. Gupta, J. C. Mikovitz and T. Zhang, 2006: The NASA/GEWEX Surface Radiation Budget project: Overview and analysis. *Extended Abstracts, 12th Conf. on Atmospheric Radiation*, Madison, WI, Amer. Meteor. Soc., 10.1.

Gupta, S. K., P. W. Stackhouse, S. J. Cox, J. C. Mikovitz, and T. Zhang, 2006: Surface Radiation Budget Project completes 22-year data set, *GEWEX News*, Vol. 16, no. 4, International GEWEX Project Office, Silver Spring, MD, 12-13.

Rossow, W. B., and R. A. Schiffer, 1991: ISCCP cloud data products. *Bull. Amer. Meteor. Soc.*, **72**, 2-20.

Trenberth, K. E., J. T. Fasullo, and J. Kiehl, 2009: Earth's global energy budget. *Bull. Amer. Meteor. Soc.*, **90**, 311-323.

Wilber, A. C., G. L. Smith, S. K. Gupta, and P. W. Stackhouse, 2006: Annual cycles of surface shortwave radiative fluxes. *J. Climate*, **19**, 535-547.